J Mater Sci (2009) 44:4148–4154
DOI 10.1007/s10853-009-3608-3

TEM characterization of iron-oxide-coated ceramic membranes

B. S. Karnik · M. J. Baumann · L. M. Corneal · S. J. Masten · S. H. Davies

Received: 27 February 2009 / Accepted: 16 May 2009 / Published online: 2 June 2009

Abstract Commercially available porous alumina–zirconia–titania ceramic (AZTC) membranes having a titania surface coating were characterized using transmission electron microscopy (TEM), X-ray diffraction (XRD), and the Brunauer–Emmett–Teller (BET) method. TEM photomicrographs showed the as-received AZTC membrane to be a multi-layered structure consisting of a porous alumina–zirconia–titania core having ultrafine pore sizes, coated by an additional layer of nanoporous titania. Electron diffraction studies revealed an amorphous surface titania layer while the underlying AZTC membrane was crystalline. The AZTC membranes were coated 20, 30, 40, 45, or 60 times with iron oxide (Fe_2O_3) nanoparticles, after which the membranes were sintered in air at 900 °C for 30 min. TEM revealed a relatively uniform nanoporous Fe_2O_3 coating on the sintered, coated membranes, where the Fe_2O_3 coating thickness increased with increasing number of layers. Electron diffraction patterns showed the Fe_2O_3 coating to be crystalline in nature. This was confirmed by the XRD results showing the structure to be α-Fe_2O_3, while the AZTC membrane was a mixture of the anatase and rutile phase of TiO_2 as well as ZrO_2 and corundum, Al_2O_3. The average pore size of the underlying AZTC membrane increased after the Fe_2O_3-coated membrane was sintered. The nanoporosity in the sintered Fe_2O_3 coating increased until 40 layers, beyond which no significant increases in the average pore size were observed. The iron-oxide-coated membrane improved catalytic properties when used in combination with ozone to treat water. The optimal benefit, in terms of water treatment efficacy, was found at 40 layers of Fe_2O_3.

B. S. Karnik
Malcolm Pirnie, Inc., 1700 West Loop South, Suite #1450, Houston, TX 77027, USA

M. J. Baumann · L. M. Corneal (✉)
Department of Chemical Engineering & Materials Science, Michigan State University, East Lansing, MI 48824, USA
e-mail: wrigh296@msu.edu

S. J. Masten · S. H. Davies
Department of Civil & Environmental Engineering, Michigan State University, East Lansing, MI 48824, USA

Introduction

The use of ceramics as catalyst materials is a well-accepted practice [1] and has led to the development of ceramic materials that are effective catalyst supports and catalytic agents. Recent advances in our ability to manipulate structures at the molecular and atomic levels have further advanced the use of nanosized ceramics as catalytic materials [1, 2]. Ceramic catalysts are used in the production of commodity chemicals and pharmaceuticals, and are finding increased application in environmental pollution control and abatement [1, 3]. Mixed metal oxides have displayed promising catalytic properties in addition to improved structural and acid–base properties [4].

Membrane filtration is an effective technique for the removal of particulate matter, micro-organisms, and organic matter from water [5]. During recent years, there has been increasing interest in the application of micro porous ceramic membranes because of their chemical, mechanical, and thermal stability [6]. The use of ozone in combination with polymeric membrane filtration has had limited success

[7–10]. In contrast to polymeric membranes, ceramic membranes are ozone resistant and when used in combination with ozone, stable permeate fluxes can be achieved without membrane damage [11–16].

Our earlier work showed that stable permeate fluxes could be maintained using uncoated alumina–zirconia–titania ceramic (AZTC) membranes in a combined ozonation–membrane filtration process [11]. Further, combined ozonation and membrane filtration resulted in a decrease in the concentration of disinfection by-products (DBPs), such as total trihalomethanes (TTHMs) and halo acetic acids (HAAs), of up to 80% and 65%, respectively. This results from the formation of partially oxidized compounds from natural organic matter (NOM) that were less reactive with chlorine [17]. Using a combined ozonation–membrane filtration system, where the AZTC membranes were coated with Fe_2O_3 nanoparticles, a further reduction of at least 50% was measured when compared to the combined ozonation and uncoated AZTC membrane filtration system. A 5-kDa nominal molecular weight cut-off (MWCO) AZTC membrane, coated with 40 layers of Fe_2O_3 nanoparticles and sintered in air at 900 °C, combined with ozonation (at a gaseous ozone concentration of 2.5 g/m^3) was able to effectively treat water from a borderline eutrophic lake (total organic carbon (TOC): 10-12 mg/L). The product water met the US EPA regulatory requirements for TTHMs of 80 μg/L and HAAs of 60 μg/L set under the Stage 2 D/DBPs Rule for drinking water [18, 19]. Subsequent research has examined the mechanisms for the degradation of NOM and the removal of harmful DBPs by the iron-oxide-coated AZTC ceramic membranes [20].

The effects of sintering temperature and coating layer thickness on the microstructure of the commercially available AZTC membranes coated with sol suspension processed Fe_2O_3 nanoparticles have been characterized in our laboratory using atomic force microscopy (AFM), scanning electron microscopy (SEM), and energy dispersive X-ray spectroscopy (EDS) [21]. These results showed a decreasing surface roughness after Fe_2O_3 coating, while an increase in the Fe_2O_3 coating thickness caused a change in the microstructure from a fine-grained morphology at 20 coating layers (average grain size 27 ± 10 nm) to a coarser grained morphology at 40 coating layers (average grain size 66 ± 23 nm) with a corresponding increase in the average pore size from 57 ± 15 to 120 ± 40 nm. Optimum water quality was achieved at a coating of 40 layers of Fe_2O_3, corresponding to a surface having a uniform, coarse-grained (average grain size 66 ± 23 nm) structure with open, nanosized (66 ± 23 nm) interconnected pores [21].

In this work, transmission electron microscopy (TEM) and X-ray diffraction (XRD) were used to further investigate the characteristics of the Fe_2O_3 nanoparticle-coated AZTC membranes.

Experimental

Membrane preparation

Tubular AZTC (a mixture of alumina, zirconia, and titania) membranes (CéRAM Inside, TAMI North America, St. Laurent, Québec, Canada, shown in Fig. 1) with a cloverleaf (three channel) design, with a nominal MWCO of 5 kDa, were used as a support for the Fe_2O_3 catalytic coatings. The external diameter of each membrane was 1 cm and the active membrane length was 8 cm. The total filtering area of each membrane was approximately 11 cm^2. The initial permeability of the membranes was determined using distilled deionized (DDI) water [11].

A detailed description of the membrane preparation is available in our earlier published work [18]. The colloidal Fe_2O_3 nanoparticles used for coating ceramic membranes were prepared by rapid hydrolysis of ferric chloride in boiling water using Sorum's method [22]. TEM characterization of the Fe_2O_3 nanoparticles showed that the average particle diameter was 4–6 nm (Fig. 2). The layer-by-layer technique used to coat the AZTC membranes is based on a protocol described by McKenzie et al. [22] for coating doped tin oxide electrodes. The AZTC membranes were immersed in the colloidal suspensions for 1 min and then rinsed with DDI water. The membranes were then immersed in aqueous phytic acid (40 mM) for 1 min and again rinsed with DDI water. This sequence was repeated for the desired number of times (20, 30, 40, 45, or 60). After coating, the Fe_2O_3-coated AZTC membranes were sintered in air at 900 °C for 30 min. This temperature was chosen to produce membranes on which the Fe_2O_3 particles were sintered together as well as to the underlying AZTC membrane surface. These sintered membranes were then prepared for examination using TEM and XRD.

Membrane characterization

A schematic representation of the procedure used to obtain images of the coated surface of the tubular Fe_2O_3-coated AZTC membranes is given in Fig. 1. The membrane was first sliced into circular discs of 1-mm thickness using a diamond-wafering saw. Subsequently, these 1-mm sections were sliced with a razor blade to form small arcs, 3 mm in length, and 1 mm in width. These arcs were mounted onto slotted copper grids, (3-mm inner diameter) perpendicular to the slot. The grids were then subsequently mounted on stubs for further preparation.

The grids were next prethinned with hand polishing using 15, 6, 3, and then 1 μm diamond paste to obtain a slice with a final thickness of approximately 70–100 μm. The samples were dimpled (GATAN Precision Dimple Grinder, Model 656) to thin the center of each disc, while

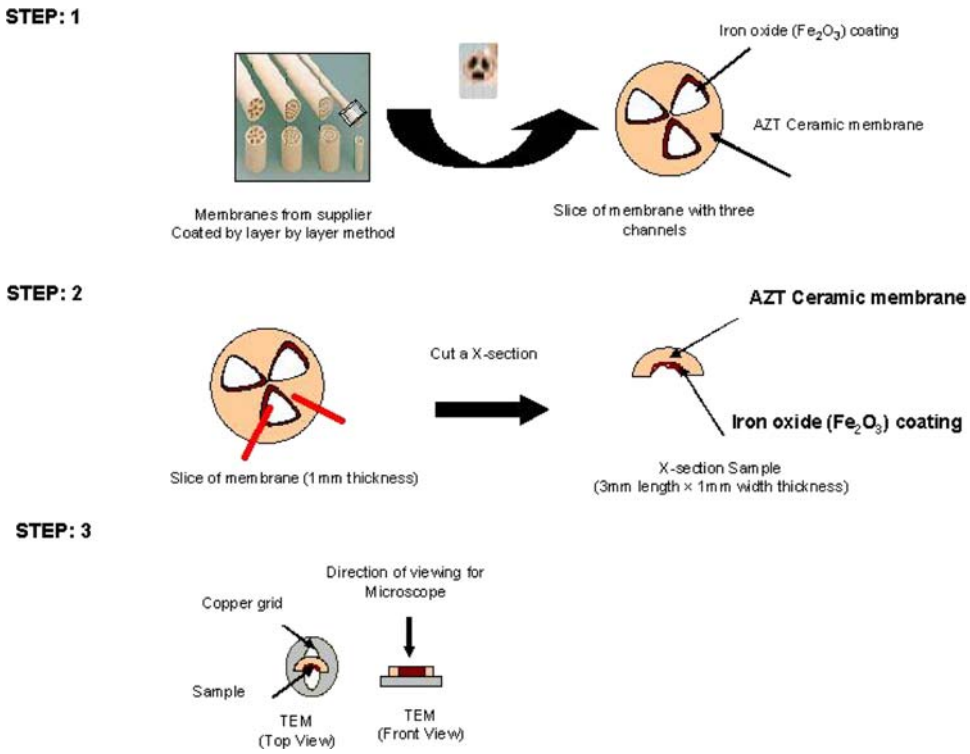

Fig. 1 Schematic representation of sample preparation for TEM imaging. With kind permission from Springer Science+Business Media: [21, p. 6863, Fig. 1]

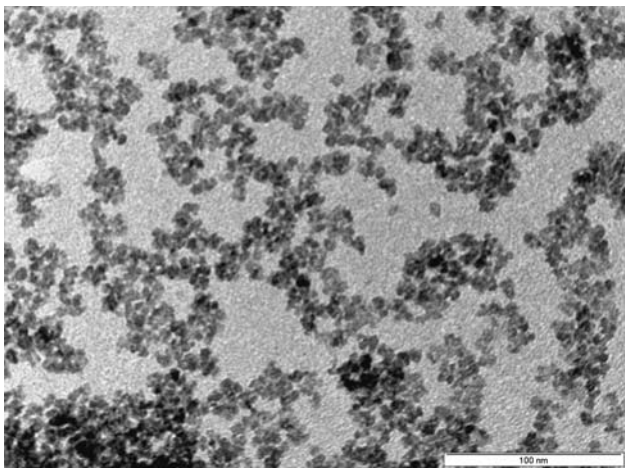

Fig. 2 TEM image of Fe_2O_3 nanoparticles processed from sol suspension (supported on holey carbon film)

minimizing the damage to the sample surface. The dimpler load was controlled and approximately 40 μm of sample removed, making the final thickness approximately 40–60 μm. The final thinning of the Fe_2O_3-coated ceramic membranes was done by ion milling, at an accelerating voltage of 4.5 keV with ion beam inclination of 4°, to avoid preferential thinning, using a commercial ion mill (GATAN Precision Polishing System Model 691). The thinned specimens were examined using TEM on a JEOL 2200FS at accelerating voltage of 200 kV and photomicrographs collected using a Hamamatsu CCD digital camera. Selected area diffraction patterns, using a nano-aperture of 100 nm in diameter, were collected at a camera length of 100 cm in order to characterize the Fe_2O_3 surface layer.

X-ray diffraction analysis using Cu Kα radiation was carried out on a Rigaku Rotaflex 200B diffractometer at an accelerating voltage of 45 kV and a current of 100 mA. Samples were scanned at angles ranging from 20° to 80°, with a scanning angle speed of 2°/min, and a step size of 0.02°, and the results were analyzed using MDI Jade 6.5 XRD software.

Nitrogen adsorption–desorption isotherms were recorded on a NOVA 2000. The samples of size 1 cm × 1 cm weighing 1.2 ± 0.05 g were dried at 150 °C under vacuum overnight, prior to nitrogen gas sorption measurement. The specific surface area was calculated using the multipoint Brunauer–Emmett–Teller (BET) method [23]. Pore size distributions were calculated by the Barrett, Joyner, and Halenda (BJH) method [24].

Results and discussion

Figure 3a is a TEM photomicrograph of a cross-section of an as-received AZTC membrane. This micrograph reveals a multi-layered structure showing the underlying AZTC membrane with a TiO_2 filtration coating.

After coating the AZTC membranes with 40 layers of Fe_2O_3 nanoparticles, TEM photomicrographs clearly show

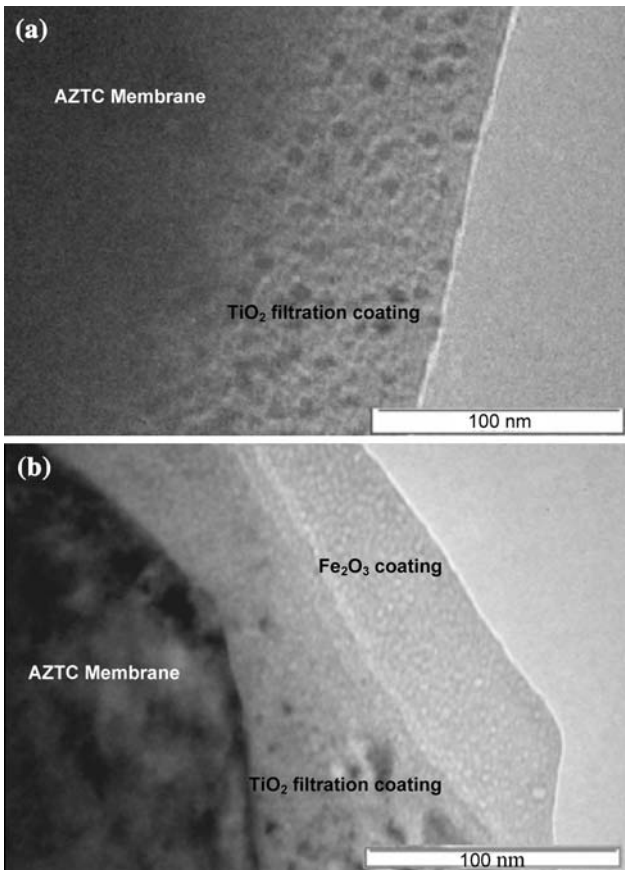

Fig. 3 **a** TEM cross-section of the micro porous AZTC membrane supplied from the manufacturer. **b** TEM cross-section of micro porous AZTC membrane with 40 layers of iron oxide sintered at 900 °C for 30 min

a second distinct surface layer (Fig. 3b) having an average thickness of ~46 nm. The electron diffraction pattern of this coating (shown in the inset of Fig. 4) demonstrates the crystalline nature of this hexagonal closed packed (hcp) α-Fe_2O_3 coating.

While not clear from the TEM micrographs, evidence of Fe_2O_3 diffusion into the porous AZTC membrane was demonstrated using EDS mapping in the SEM, which clearly showed that iron had diffused into the membrane to a depth of at least 500 μm (Fig. 4) [21].

Figures 5, 6, and 7 illustrate the relationship between the number of times the membrane was coated with Fe_2O_3 and the resulting thickness of the sintered apparent surface Fe_2O_3 coating, as well as the continued crystalline nature of the Fe_2O_3 coating. Since the water quality improvements were most significant with membranes coated with 40, 45, and 60 layers, these were the samples that were used for TEM characterization. While the TEM photomicrograph for 40 layers of Fe_2O_3 (Fig. 5) shows an Fe_2O_3 coating thickness of ~46 nm, the 45 and 60 layers of Fe_2O_3 coating (Figs. 6, 7) yielded a coating thickness of ~55 and ~57 nm, respectively. These measurements are an approximation since the exact thickness of the coatings cannot be determined because of specimen tilt as well as any damage to the TEM samples during preparation that may have removed material [25]. That being the case, in general, the coating thickness increased with increasing number of layers. The increase in the thickness of the Fe_2O_3 coating is not as large as would be expected if each layer resulted in the deposition of a complete Fe_2O_3 monolayer, given the size of the Fe_2O_3 particles (4–6 nm). If the particles were deposited in a close-packed arrangement, the expected thickness of the iron-oxide layer would be 28–42 nm for every 10 layers applied. However, from the aforementioned EDS results, we know that some of the Fe_2O_3 nanoparticles penetrated into the membrane [21]. This could be the result of capillary action through the abundant surface connected porosity during the coating process and/or further diffusion of Fe_2O_3 into the membrane during sintering [21]. Shrinkages of 40–50% are also common during sintering of ceramic powders [26]. Therefore, it is reasonable to achieve a ~46-nm thick coating, for 40 applied layers of Fe_2O_3, after taking into account the combined effects of diffusion into the interior of the membrane and sintering shrinkage.

Water quality data for AZTC membranes coated 0, 20, 30, 40, 45, and 60 times are shown in Fig. 8. More detailed presentations of these water quality results have been

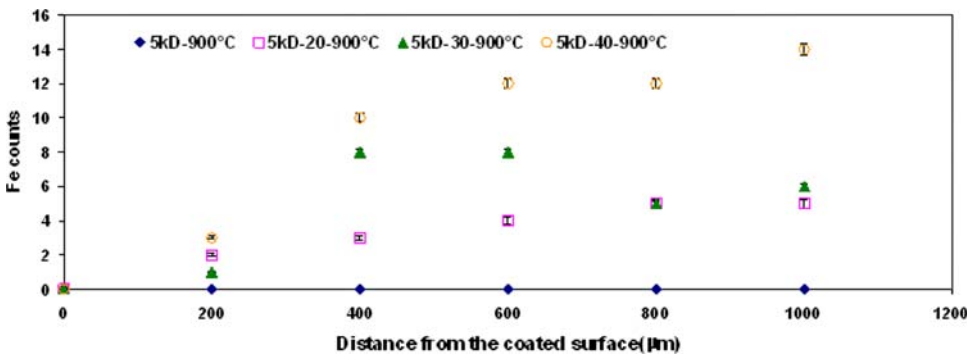

Fig. 4 Relative Fe concentration from EDS scans. The graph represents relative Fe concentrations measured as Fe counts in the EDS scans. With kind permission from Springer Science+Business Media: [21, p. 6869, Fig. 10]

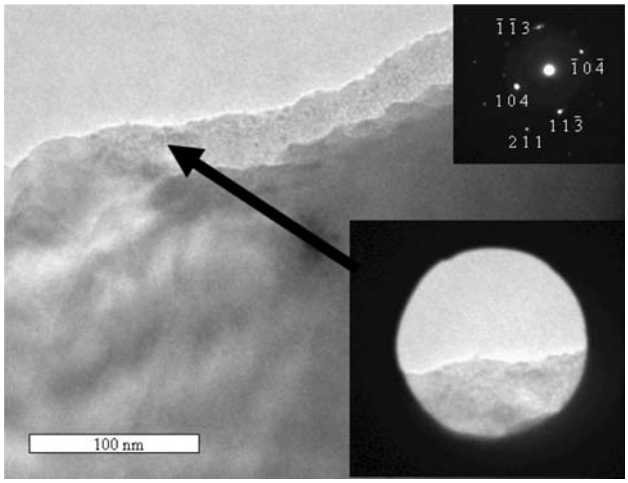

Fig. 5 TEM cross-section of the porous AZTC membrane with 40 layers of iron oxide sintered at 900 °C for 30 min with the selected area diffraction aperture size of 100 nm with the corresponding diffraction pattern demonstrating the crystalline nature of the sintered iron oxide coating. The *bar scale* represents 100 nm

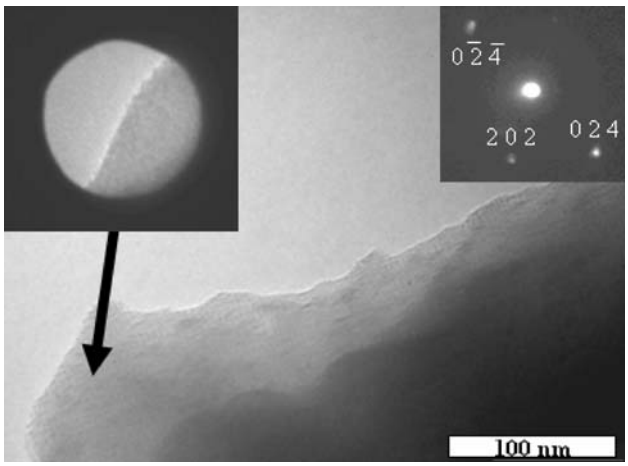

Fig. 6 TEM cross-section of coated 5-kDa AZTC membrane with 45 layers of iron oxide, sintered at 900 °C for 30 min

published elsewhere [11, 17, 18, 21]. AZTC membrane performance in terms of water quality improved as the thickness of the catalytic layer increased. This may occur because as the coating thickness increased, a greater surface area is available to facilitate surface catalytic reactions that result in the degradation of contaminants in the treated water. Comparing water quality data for the AZTC membranes coated 20 and 30 times shows no statistically significant differences in terms of water quality for the two membranes, which may be linked to similar sintered coating Fe_2O_3 thicknesses for these two membranes. For the membrane coated 40 times, the sintered Fe_2O_3 coating thickness increases, and we find a corresponding improvement in water quality. However, 40 Fe_2O_3 coating layers was found to be the optimum in terms of water

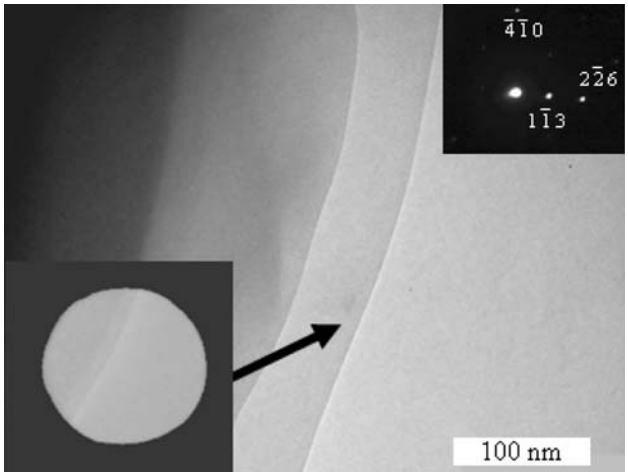

Fig. 7 TEM cross-section of coated 5-kDa AZTC membrane with 60 layers of iron oxide, sintered at 900 °C for 30 min

quality improvements, as membranes coated 45 and 60 times showed no further gains in performance. Again, the fact that the membranes coated with 45 or 60 Fe_2O_3 layers also showed little or no gain in performance may be related to the small increase in the Fe_2O_3 surface thickness compared to that for the membrane coated 40 times.

Diffusion of Fe_2O_3 into the AZTC membrane also has long-term implications for the successful commercialization of this technology because over time, the coating on the surface of the ceramic membrane may gradually erode or become coated with surface deposits. The benefits of the catalytic action of the Fe_2O_3 would be expected to continue as the iron-oxide particles found in the interior of the membrane react with the dissolved ozone present in the water, which permeates through the filtration and support layers of the membrane.

X-ray diffraction characterization (Fig. 9) of the samples showed that the uncoated, unsintered AZTC membrane samples as well as the uncoated AZTC membrane samples sintered in air at 900 °C were a mixture of the anatase and rutile phase of TiO_2 as well as ZrO_2 and corundum, Al_2O_3. Following coating, the XRD scans showed the presence of α-Fe_2O_3 with no changes observed after sintering in air at 900 °C. All XRD peaks were indexed as hcp α-Fe_2O_3 with a least squares best fit lattice parameter of 0.5036 ± 0.0002 and 1.3752 ± 0.0002 nm.

The surface area and pore size measurements for the samples are tabulated in Table 1. The BET surface area measurements did not show any statistically significant difference in surface area as a function of number of Fe_2O_3 layers. The pore size distributions show the average pore size of 4.61 ± 0.02 nm for the as-received AZTC membrane. The pore size increased slightly upon sintering to 4.80 ± 0.03 nm. For both the 20 and 30 Fe_2O_3 layer-coated AZTC membranes, the average pore size was

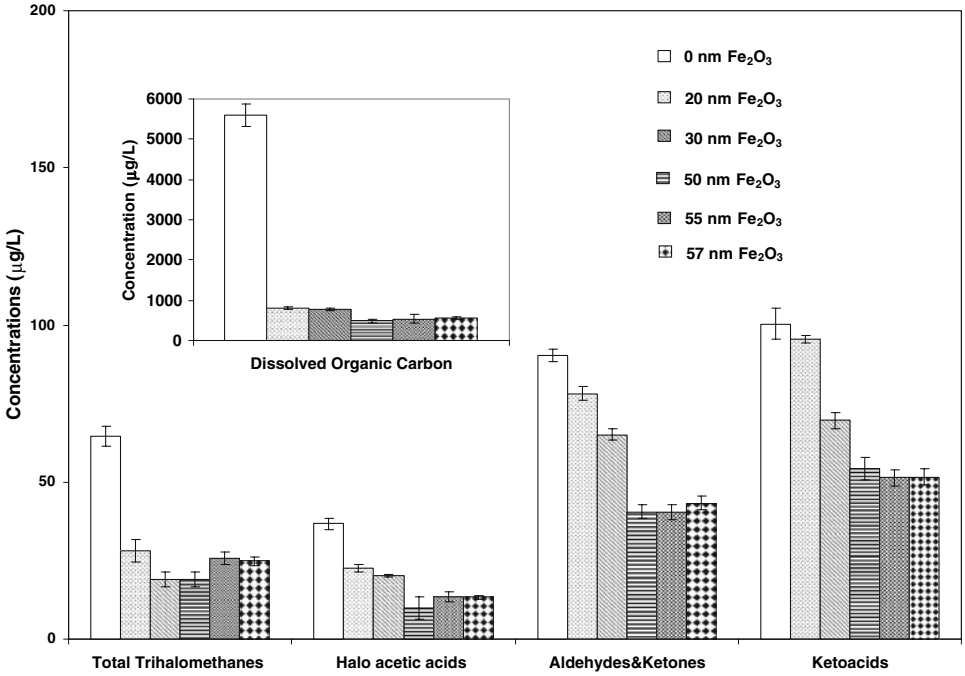

Fig. 8 Water quality data for the permeate after the combined ozonation–membrane treatment process. The data for water quality parameters for a 5-kDa AZTC membrane uncoated, unsintered (0-nm coating thickness), with 20, 30, 40, 45, and 60 layers of iron oxide, sintered at 900 °C for 30 min with, respectively, 20, 30, 50, 55, 57 nm coating thickness. The inset in the graph is the plot of dissolved organic carbon concentrations for the same membranes. Experiment details [18, 21]. With kind permission from Springer Science+Business Media: [21, p. 6869, Fig. 11]

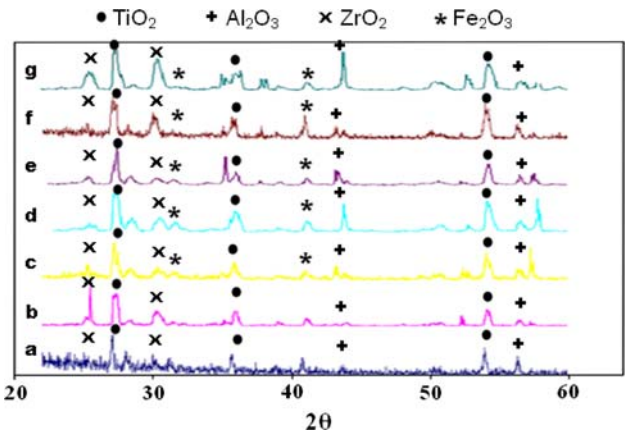

Fig. 9 X-ray diffraction patterns of AZTC membrane, (a) 5-kDa MWCO AZTC membrane uncoated, (b) 5-kDa AZTC membrane uncoated, sintered at 900 °C for 30 min, (c) 5-kDa AZTC membrane with 40 layers of iron oxide unsintered and (d–g) 5-kDa AZTC membrane with 20, 30, 40, or 45 layers of iron oxide, sintered at 900 °C for 30 min

4.80 nm, but beyond 30 Fe_2O_3 layers, the average pore size increased to 5.20 nm. It should be further noted that the additional heat treatment required to sinter the Fe_2O_3 layers also serves to coarsen the pores in the underlying AZTC membrane. These results suggest that increasing the number of Fe_2O_3 layers yields a corresponding increase in coarsening, which facilitates the catalytic performance, as well as transforming the surface from a relatively flat surface to one having surface undulations at the micron scale. This confirms our earlier AFM results showing a decrease in submicron scale surface roughness with sintering and Fe_2O_3 coating [18, 21]. We did not find any statistically significant decrease in AFM roughness beyond 40 layers, as shown in our previous AFM analysis [21]. Further these TEM photomicrographs confirm, as do our other findings, that the sintered Fe_2O_3-coated AZTC membranes used in our hybrid nanofiltration–ozonation study are indeed still operating with nanoscale porosity.

Conclusions

Transmission electron microscopy observations revealed that coating the AZTC membrane with iron-oxide nanoparticles followed by sintering at 900 °C in air resulted in a nanosized crystalline α-Fe_2O_3 surface layer. Increasing the number of Fe_2O_3 layers did not produce a corresponding one-to-one increase in the thickness of the Fe_2O_3 coating. The fact that the thickness of the coating is less than might be expected is most likely due to both movement of the Fe_2O_3 nanoparticles into the membrane by capillary action and subsequent diffusion during densification of the porous Fe_2O_3 layers during sintering.

Brunauer–Emmett–Teller measurements showed that the average pore size increased with increasing number of Fe_2O_3 coating layers. This coarsening of the pores corresponds with the improved catalytic performance of the membranes, which was optimal for the membrane coated 40 times with Fe_2O_3 particles. Capillary action during the coating process, and/or diffusion during sintering, resulted in a uniform distribution of iron-oxide particles into the membrane to a depth of at least 500 μm. The synergy of

Table 1 Summary of surface area and average pore size

Sample	Surface area (m^2/g)	Average pore size (nm)
5 kDa—uncoated—unsintered	4.99 (±0.05)	4.61 (±0.02)
5 kDa—20 layers—900 °C	5.12 (±0.05)	4.80 (±0.03)
5 kDa—30 layers—900 °C	5.17 (±0.05)	4.80 (±0.02)
5 kDa—40 layers—900 °C	4.45 (±0.05)	5.13 (±0.03)
5 kDa—45 layers—900 °C	4.52 (±0.05)	5.20 (±0.01)
5 kDa—60 layers—900 °C	4.59 (±0.05)	5.20 (±0.02)

the catalytic effect of the Fe_2O_3 nanoparticle coating on the membrane surface and the diffused Fe_2O_3 particles within the membrane enhances the performance of the combined ozone–membrane filtration process, because of the increased exposure to the catalytic iron oxide, not only at the membrane surface, but into the membrane itself. The quality of the water filtered by the process exceeds the current EPA regulatory requirements [19].

Acknowledgements The authors would like to acknowledge the US Environmental Protection Agency (US EPA) Science to Achieve Results (STAR) Program (Grant No. RD830090801) and the National Science Foundation Nanoscale Interdisciplinary Research Teams (NSF-NIRT) Program (Grant No. BES0506828) for financial support of this work. Our thanks also go to Ms. Alicia Pastor, from the Center for Advanced Microscopy and Mr. Robert Pcionek for there assistance during TEM sample analysis. Mr. Rui Huang is also acknowledged for XRD analysis of the samples. Thanks are due to Yang Chen for performing the BET measurements. We would also like to thank Mr. David Jackson for his assistance with the membrane coating process. Finally, we gratefully acknowledge the helpful suggestions and comments from Prof. G.M. Janowski of the University of Alabama at Birmingham.

References

1. Keane MA (2003) J Mater Sci 38:4661. doi:10.1023/A:1027406515132
2. Trudeau ML, Ying JY (1996) Nanostruct Mater 7:245
3. Onda A, Suzuki Y, Takemasa S, Kajiyoshi K, Yanagisawa K (2008) J Mater Sci 43:4230. doi:10.1007/s10853-008-2612-3
4. Neri G, Rizzo G, Galvagno S, Loiacono G, Donato A, Musolino MG, Pietropaolo R, Rombi E (2004) Appl Catal A 274:243
5. US EPA (2001) In Low-pressure membrane filtration for pathogen removal: application, implementation and regulatory issues. Office of Water 815-C-01-001
6. Puhlfürß P, Voigt A, Weber R, Morbé M (2000) J Membr Sci 174:123
7. Hashino M, Mori Y, Fujii Y, Motoyama N, Kadokawa N, Hoshikawa H, Nishijima W, Okada M (2000) Water Sci Technol 41:17
8. Shanbhag PV, Guha AK, Sirkar KK (1998) Ind Eng Chem Res 37:4388
9. Castro K, Zander AK (1995) J Am Water Works Assoc 87:50
10. Shen ZS, Semmens MJ, Collins AG (1990) Environ Technol 11:597
11. Karnik BS, Davies SHR, Chen KC, Jaglowski DR, Baumann MJ, Masten SJ (2005) Water Res 39:728
12. Schlichter B, Mavrov V, Chmiel H (2004) Desalination 168:307
13. Allemane H, Deloune B, Paillard H, Legube B (1993) Ozone Sci Eng 15:419
14. Kim JO, Somiya I (2001) Environ Technol 22:7
15. Kim JO, Somiya I, Fujii S (1991) In: Proceedings of the 14th Ozone World Congress. Dearborn, MI, p 131
16. Sartor M, Schlichter B, Gatjal H, Mavrov V (2008) Desalination 222:528
17. Karnik BS, Davies SH, Baumann MJ, Masten SJ (2005) Water Res 39:2839
18. Karnik BS, Davies SH, Baumann MJ, Masten SJ (2005) Environ Sci Technol 39:7656
19. List of drinking water contaminants and MCLS (2009) EPA website. http://www.epa.gov/safewater/mcl.html#mcls. Accessed 27 May 2009
20. Karnik BS, Davies SH, Baumann MJ, Masten SJ (2007) Environ Eng Sci 24:852
21. Karnik BS, Baumann MJ, Masten SJ, Davies SH (2006) J Mater Sci 41:6861. doi:10.1007/s10853-006-0943-5
22. McKenzie KJ, Marken F, Hyde M, Compton RG (2002) New J Chem 26:625
23. Brunauer S, Emmett PH, Teller E (1938) J Am Chem Soc 60:309
24. Barrett EP, Joyner LG, Halenda PP (1951) J Am Chem Soc 73:373
25. Williams DB, Carter CB (1996) In: Transmission electron microscopy. Springer, New York, p 187
26. Barsoum MW (2003) In: Cantor B, Goringe MJ (eds) Fundamentals of ceramics. Institute of Physics Publishing, Bristol, p 307